Effects of Formulation and Processing Variables on the Rheology of Chitosan–Vanillin Stabilized Olive Oil–Water Emulsions for Oleogel Applications

Leticia Montes , David Rey , Ramón Moreira , Daniel Franco *

Posted Date: 27 February 2026

doi: 10.20944/preprints202602.1360.v1

Keywords: chitosan-vanillin oleogels; interfacial structuring; Herschel-Bulkley rheology; Schiff base crosslinking; yield stress; thermal stability

 doi:10.20944/preprints202602.1360.v1

Article

Effects of Formulation and Processing Variables on the Rheology of Chitosan–Vanillin Stabilized Olive Oil–Water Emulsions for Oleogel Applications

Leticia Montes, David Rey, Ramón Moreira and Daniel Franco *

Department of Chemical Engineering, Universidade de Santiago de Compostela, rúa Lope Gómez de Marzoa, s/n, 15782 Santiago de Compostela, Spain

* Correspondence: daniel.franco.ruiz@usc.es

Abstract

The rheological behavior of chitosan–vanillin crosslinked olive oil–in–water emulsions (Φ=0.52) was systematically studied as a function of key processing (homogenization time and speed, reaction temperature) and compositional variables (chitosan concentration, vanillin-to-chitosan molar ratio, and Tween® surfactant) to optimize their performance as oleogel precursors. All emulsions displayed viscous-dominant behavior, with a characteristic inflection in the storage modulus slope at ~0.1 Hz, except for Tween®-containing systems, which superimposable flow curves confirmed non-thixotropic Herschel–Bulkley pseudoplastic behavior (n ≈ 0.73) was observed. Optimal homogenization conditions (4 min, ≥ 9,500 rpm) promoted microstructural refinement without compromising emulsion stability. Increasing reaction temperature to 55 °C, approaching the chitosan percolation threshold (~0.8–0.9% w/w), and a vanillin-to-chitosan molar ratio of 0.7 maximized yield stress (up to 14.21 Pa), consistency, and thermal robustness, attributed to enhanced Schiff-base crosslinking and network densification. Tween® 20 and Tween® 60 induced oscillatory stiffening but caused pronounced softening under rotational shear due to interfacial displacement effects, with Tween® 20 providing superior thermal stability. Overall, a surfactant-free formulation (0.9% w/w chitosan, molar ratio 0.7, 55 °C) yielded highly structured, gel-like emulsions, demonstrating enhanced suitability as templates for olive oil oleogel development compared to conventional stabilization strategies.

Keywords: chitosan-vanillin oleogels; interfacial structuring; Herschel-Bulkley rheology; Schiff base crosslinking; yield stress; thermal stability

1. Introduction

The replacement of saturated (SFA) and trans fats (TFA) with healthier alternatives has become a critical priority in food innovation due to the well-established relationship between these types of fats and the increased risk of cardiovascular and metabolic diseases. SFA, mostly found in animal products, and TFA, often present in processed foods, are linked to elevated cholesterol levels and systemic inflammation that contribute to chronic health conditions [1]. Vegetable oils, which are predominantly liquid at room temperature, usually offer beneficial fatty acid compositions, especially rich in mono- and polyunsaturated fatty acids with positive effects on human metabolism [2]. However, their liquid state limits their direct use as replacements for solid animal fats in products that require specific textures and stability. Consequently, the structuring of liquid vegetable oils into semi-solid networks resembling animal fats has attracted great scientific and industrial interest, boosting the development of structuring strategies to convert liquid oils into semi-solid systems, such as oleogels, that resemble animal fats in technological performance. Oleogels are emerging semi-solid systems in which liquid vegetable oils are immobilized within a three-dimensional network formed by structuring agents such as polymers or low-molecular-weight compounds [3]. These networks

 doi:10.20944/preprints202602.1360.v1

impart mechanical stability while mimicking the texture and mouthfeel of conventional solid fats. Among the different structuring strategies, the emulsion-template approach has gained considerable attention due to its versatility in structuring oils using hydrophilic biopolymers, including polysaccharides and proteins [4]. In this method, an oil-in-water emulsion is first prepared with the structuring agent dissolved in the aqueous phase; subsequent removal of water by drying yields a continuous solid matrix that entraps the oil droplets within the polymeric network [3,5]. Consequently, the microstructural features of the initial emulsion—such as droplet size, spatial organization, and stability—play a decisive role in determining the properties of the resulting oleogel. The formation of stable emulsion templates, however, remains technically challenging, as destabilization phenomena including coalescence, creaming, or phase separation must be carefully controlled to preserve structural integrity [6]. Emulsion structure is governed by a complex interplay of processing parameters (e.g., homogenization intensity and duration, thermal history) and formulation variables (e.g., gelator concentration, oil volume fraction, component ratios, and the presence of surfactants or emulsifiers. Because the final oleogel largely inherits the droplet packing and continuous-phase connectivity established in the parent emulsion, a rigorous evaluation of how these variables affect emulsion structure is essential. In this context, rheology provides a particularly powerful and sensitive tool, as it quantitatively reflects microstructural organization and has been proposed as a predictive descriptor for the manufacture and performance of highly structured emulsions [7]. Nevertheless, despite the growing interest in emulsion-templated oleogels, systematic studies linking processing and formulation variables to emulsion rheology, and subsequently to oleogel properties after dehydration, remain scarce. Instead, many studies rely on processing conditions adopted from previous work, often without rheological justification for their suitability in specific biopolymer–surfactant systems, thereby limiting reproducibility and rational scale-up. Addressing this gap through controlled, multivariable rheological investigations is therefore crucial for the rational design of emulsion templates capable of yielding robust and reproducible oleogels.

Chitosan, a bio-based polysaccharide derived from chitin found abundantly in crustacean shells, offers an attractive option as a structuring agent due to its biodegradability and biocompatibility [8]. Vanillin, widely used industrially as a flavoring agent, possesses functional groups capable of forming covalent and hydrogen bonds with chitosan, thus reinforcing the polymeric network [9]. The Schiff base reaction between primary amines of chitosan and the aldehyde group of vanillin produces a crosslinked structure helping to improve the mechanical and functional properties of the system.

Specifically, recent literature on chitosan-based oleogels reveals substantial variability in the conditions used to prepare the initial emulsions. Most studies employ high-shear mechanical homogenization—typically using Ultra-Turrax or equivalent devices—to generate oil-in-water (O/W) emulsions, with reported homogenization times ranging from 2 to 4 min and rotational speeds between 9,000 and 15,000 rpm [10–15] or even milder conditions such as 30 min and 600 rpm [16]. Such differences might have important implications for reproducibility and represent a major limitation for translating these systems to larger scale processes. Emulsification is generally performed under mild, non thermal conditions; however, temperature is a critical factor in the Schiff base reaction, and its effects on emulsion stability remain unexplored. Moreover, nearly all studies rely on freeze drying (i.e -40 -60 °C) as the dehydration method, except Lin et al. [10]. Regarding compositional variables, chitosan concentration is the most consistently reported parameter, as it is widely recognized as a key structuring factor. Nonetheless, chitosan based formulations are typically restricted to a narrow concentration window (~0.7–3% w/v), and different studies use non standardized units making direct comparisons difficult without additional assumptions or recalculations. Vanillin is universally described as a Schiff base crosslinker because crosslinking is central to oleogel formation and stability; yet none of the available studies explicitly reports the vanillin to chitosan molar ratio. Notably, at least two works [10,13] do not employ the Schiff reaction, achieving structuring through glycyrrhizic acid [10] or whey protein isolate [13]. These differences prevent mechanistic comparison of crosslinking density, representing a significant knowledge gap, particularly for establishing structure–property relationships. Finally, some of the aforementioned

 doi:10.20944/preprints202602.1360.v1

studies rely on biopolymer-based interfacial stabilisation, while others selectively incorporate Tween® 60 to enhance emulsification efficiency.

Overall, emulsification is treated as a preparative step rather than a controlled process variable. Consequently, key kinetic and mechanical parameters—such as homogenization time, shear rate, temperature, and molar ratios—are systematically underreported, despite their known influence on droplet size, interfacial organization, and the final structure of the oleogel. Therefore, this study investigates olive oil–water emulsions stabilized by chitosan and vanillin as a critical intermediate in oleogel production, to systematically evaluate the influence of critical operational variables on emulsion stability and mechanical properties. Based on this analysis, an optimized protocol is proposed to obtain reproducible, kinetically stable emulsions with strong potential for application as healthier, functional fat replacers in food formulations.

2. Materials and Methods

2.1. Materials

Medium-molecular-weight chitosan was purchased from Sigma-Aldrich (St. Louis, MO, USA). The degree of deacetylation was 75–85%, and the viscosimetric molecular weight was 300±18 Kg/mol. Food-grade olive oil was supplied by Aceites Abril SL (Ourense, Spain). Vanillin (152.15 g/mol), Tween® 20 and Tween® 60 were purchased from Sigma-Aldrich and used as received.

2.2. Preparation of Chitosan Solutions

Chitosan was dissolved in a 1% (v/v) acetic acid aqueous solution and stirred at 400 rpm at 50 °C for 2 h. pH was adjusted to 4.5 with sodium acetate buffer. Solutions were prepared at different concentrations (0.6% to 1.0% w/v).

2.3. Emulsion Preparation

Olive oil was added dropwise via burette directly through the Ultra-Turrax probe (IKA T25 basic, Germany) at the specified homogenization speeds to the chitosan solution (previously prepared at 0.6–0.9% w/v, pH 4.5) placed on an orbital shaker (P-Selecta Rotaterm, Spain) at 150 rpm. Addition occurred over 3 min, followed by a 30 s pause. Vanillin was dissolved in 96% ethanol and added over the next 30 s to achieve target molar ratios.

Secondary homogenization continued for specified times (0.5, 2, 4, or 10 min) at constant speed, with the beaker immersed in a cold-water bath for temperature control for viscous samples or extended processing. Post-homogenization, emulsions were transferred to a closed vessel and stirred magnetically (400 rpm, 2 h) at the specified reaction temperatures (25, 40, or 55 °C) to promote chitosan–vanillin cross-linking, followed by 22 h maturation at room temperature prior to analysis.

Oil-to-aqueous addition order proved critical, as reverse addition yielded phase-separated systems; the adopted oil-into-chitosan protocol followed Brito et al. [12]. Tween® 20/60 variants incorporated 0.4% w/w surfactant directly into the chitosan solution prior to identical emulsification. All formulations maintained constant oil phase volume ($\varphi \approx 0.52$) across experimental variables.

2.4. Experimental Design

The effect of processing and compositional variables on emulsion rheology and stability was investigated using a systematic experimental design. The factors considered were homogenization speed and time, emulsification temperature, chitosan concentration, vanillin-to-chitosan molar ratio and emulsifier type/level (Tween® 20 or Tween® 60). The specific levels tested for each factor are summarized in Table 1.

 doi:10.20944/preprints202602.1360.v1

Table 1. Experimental variables and tested levels for the formation of olive oil–water emulsions stabilized by chitosan and vanillin.

Experimental variable	Levels
Homogenization time (min)	0.5; 2.0; 4.0; 10.0
Homogenization speed (rpm)	6,500; 9,500; 13,500; 17,500
Reaction temperature (°C)	25; 40; 55
Chitosan concentration (% w/v)	0.6, 0.7, 0.8, 0.9, 1.0
Vanillin to chitosan molar ratio	0.0; 0.3; 0.7; 1.3
Emulsifier type	Tween® 20; Tween® 60

2.5. Rheological Characterization and Emulsion Stability

Rheological properties were determined using a controlled-stress rheometer (Anton Paar Physica MCR 301, Anton Paar, Austria) with 50 mm parallel-plate geometry and 1.5 mm fixed gap. Samples were loaded carefully, edges sealed with paraffin to prevent evaporation, and measurements conducted at 25 °C.

2.5.1. Time Sweeps

Time sweeps were performed at constant shear rate of 10 s^{-1} for 8 min to assess time-dependent behavior (thixotropy/rheopexy), confirm system stability, and verify completion of chitosan-vanillin reaction prior to subsequent tests.

2.5.2. Strain Sweeps

Strain sweeps were conducted at 1 Hz over 0.01–1000% strain to determine the linear viscoelastic region (LVR). Storage (G′) and loss (G′′) moduli remained constant below 1% strain, which was selected for all subsequent oscillatory tests.

2.5.3. Frequency Sweeps

Frequency sweeps were performed at 1% strain over 0.01–100 Hz at 25 °C to characterize viscoelastic properties and microstructural features under different processing conditions.

2.5.4. Flow Curves

Steady shear measurements were determined at different shear rates from 0.01–100 s^{-1}. Apparent viscosity data were fitted to the Herschel–Bulkley model to evaluate effects of formulation and processing variables on flow behavior. Data were fitted to the Herschel–Bulkley model, Equation (1):

$$\boldsymbol{\tau = \tau_0 + K\dot{\gamma}^n} \quad (1)$$

where τ_0 is the yield stress (Pa), K is the consistency index (Pa· s^n), and n is the flow behavior index (dimensionless).

2.5.5. Temperature Ramps

Temperature ramps (1 Hz, 1% strain) were used to assess thermal stability in selected formulations, monitoring the evolution of complex viscosity (η*) throughout the thermal cycle. Complex viscosity was calculated from the complex shear modulus as η* = G*/ω, where G* is the complex modulus obtained from oscillatory measurements and ω is the angular frequency (rad·s^{-1}).

The following temperature cycles were used: 10 min at 25 °C, heating 25–50 °C (3 °C min^{-1}), 10 min at 50 °C, cooling 50–25 °C (3 °C min^{-1}) and 10 min at 25 °C.

 doi:10.20944/preprints202602.1360.v1

2.6. Statistical Analysis

All experiments were conducted in duplicate, and results are reported as mean ± standard deviation. One-way analysis of variance (ANOVA) was performed using SPSS Statistics 29 (IBM Corp., Chicago, IL, USA) to assess the effects of independent variables on dependent responses, followed by Duncan's post-hoc test for mean separation at a significance level of $P < 0.05$. Model goodness-of-fit was evaluated using the coefficient of determination (R^2) and root mean square error (RMSE), calculated as, Equation (2):

$$\boldsymbol{RMSE} = \sqrt{\frac{\sum(\boldsymbol{X_{exp}} - \boldsymbol{X_{calc}})^2}{\boldsymbol{N} - \boldsymbol{P}}} \quad (2)$$

where X_exp and X_calc represent experimental and calculated values, respectively, N is the number of data points, and P is the number of model parameters.

3. Results and Discussion

3.1. Effect of Homogenization Time

Emulsions were prepared under constant conditions of 3 min initial mixing at 9,500 rpm (Ultra-Turrax) of the chitosan aqueous solution with olive oil, followed by vanillin addition, and orbital shaking at 150 rpm during subsequent homogenization stages. Homogenization times were varied at 0.5, 2.0, 4.0, and 10.0 min while maintaining Ultra-Turrax speed at 9,500 rpm to promote component mixing and system homogenization [17]. These processing variables directly influence continuous phase rheology, particle interactions and droplet size distribution.

3.1.1. Time Sweep

The first rheological test performed for all emulsions was a time sweep at a constant shear rate of 10 s^{-1}. This assay was used to verify the stability of the systems over time, since in the absence of ongoing molecular interactions or structural rearrangements no relevant changes in viscosity are expected during the application of a constant shear rate. Confirming this, under the conditions tested, the emulsions showed no appreciable variations in apparent viscosity, indicating that all systems were stable throughout the measurement. An increase in viscosity is primarily associated with a reduction in droplet size, since smaller droplets contribute to greater resistance to flow. In our system, longer homogenization times produced progressively higher viscosity values, which might be explained by consistent with the finer droplet size distribution generated under extended high-shear processing.

3.1.2. Strain Sweep

Strain sweeps were conducted at a constant frequency of 1 Hz to determine the linear viscoelastic region (LVR) for subsequent frequency sweep measurements. Storage (G′) and loss (G′′) moduli remained constant across the strain range tested, indicating that the systems maintained linear viscoelastic behavior, confirming that the selected strain amplitude of 1% was appropriate and within the LVR for all frequency sweep analyses.

3.1.3. Frequency Sweep

Frequency sweeps (1% strain) are shown in Figure 1A for emulsions prepared at different homogenization times. Across the entire frequency range tested, the G′′ exceeded the G′, indicating predominant viscous liquid-like behavior over elastic solid-like response, which is typical for emulsions with a dispersed phase volume fraction (Φ) below 0.56 [18]. This observation aligns with the fixed Φ = 0.52 used in this study and is consistent with previous reports on chitosan-stabilized (Hou et al., 2010) and tragacanth gum-based structured emulsions [19–21].

 doi:10.20944/preprints202602.1360.v1

The G'' values remained nearly identical across all four systems, while G' exhibited frequency-dependent differences. At low frequencies (< 0.1 Hz), G' values showed greater separation between samples, converging toward similar magnitudes at higher frequencies. Notably, G' displayed a distinct change in slope around 0.1 Hz, with a steeper increase compared to G'', suggesting a gel point (G'=G'' crossover) at higher frequencies beyond the tested range, while a second, more distant gel point appears visible at very low frequencies. The studied frequency range thus corresponds to the theoretical viscoelastic region known as the rubbery plateau or transition zone. Frequency sweep measurements revealed minimal separation of G', suggesting that shear primarily refines droplet size after network formation has been established [17].

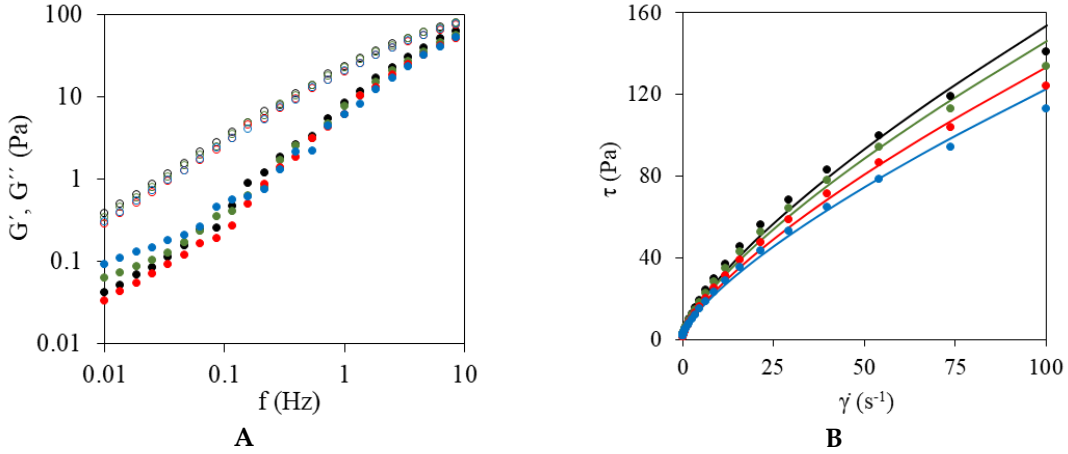

Figure 1. Effect of homogenization time on rheological properties of olive oil–water emulsions. (A) Frequency sweep: storage (G', closed symbols) and loss (G'', open symbols) moduli. (B) Flow curves: shear stress (τ) versus shear rate (γ̇) with Herschel–Bulkley model fits (lines) overlaid on experimental data (dots). Conditions: 13,500 rpm, 25 °C, 0.8% (w/v) chitosan, vanillin-to-chitosan molar ratio 0.7. Homogenization times: blue (0.5 min), red (2.0 min), green (4.0 min), black (10.0 min).

3.1.4. Flow Curve

Flow curves obtained from steady shear measurements (two cycles: one upward and one downward shear rate sweeps) are shown in Figure 1B, with Herschel-Bulkley model parameters displayed in Table 2. The flow curves for each emulsion were practically superimposable across cycles, indicating absence of significant thixotropy or structural breakdown. All systems exhibited pseudoplastic behavior (flow index, n = 0.73), with consistency index (k) increasing from 4.20 ± 0.15 Pa·s^n (0.5 min) to 5.30±0.19 Pa·s^n (10 min) and yield stress (τ_0) varying from 0.92±0.04 Pa (2 min) to 1.27±0.05 Pa (4 min). The excellent goodness of fit (RMSE = 0.004–0.087) validates the Herschel–Bulkley model and demonstrates that the structuring effect is associated with extended homogenization time. Apparent viscosity versus shear stress profiles (data not shown) exhibited a characteristic two-stage shear-thinning behavior. At low shear stress, viscosity decreased sharply with a steep slope, followed by a more gradual decline at higher stresses as the slope progressively diminished. This pattern aligns with previous observations in tragacanth gum-stabilized emulsions [19,22]).

 doi:10.20944/preprints202602.1360.v1

Table 2. Herschel-Bulkley, Equation (1), parameters of emulsions performed at different homogenization time/speed, reaction temperature, chitosan concentration, vanillin/chitosan molar ratio, and emulsifiers. τ_0 = yield stress; K = consistency index; n = flow behavior index.

Variable	Condition	τ_0 (Pa)	K (Pa·sn)	n	RMSE
Homogenization time (min)	0.5	0.94±0.06^{c}	4.20±0.15^{a}	0.73	0.087
	2.0	0.92±0.04^{a}	4.60±0.16^{b}		0.004
	4.0	1.27±0.05^{b}	5.02±0.18^{c}		0.081
	10.0	1.24±0.05^{ab}	5.30±0.19^{c}		0.071
Homogenization speed (rpm)	6,500	1.64±0.11^{c}	5.92±0.21^{b}	0.73	0.121
	9,500	1.27±0.05^{a}	5.02±0.18^{a}		0.081
	13,500	1.82±0.07^{b}	6.27±0.22^{bc}		0.059
	17,500	3.44±0.14^{d}	6.54±0.23^{c}		0.072
Reaction temperature (ºC)	25	1.27±0.05^{a}	5.02±0.18^{a}	0.73	0.081
	40	2.61±0.10^{b}	5.67±0.20^{a}		0.087
	55	2.71±0.11^{b}	5.99±0.21^{b}		0.101
Chitosan concentration (% w/w)	0.6	2.21±0.08^{b}	6.70±0.24^{b}	0.73	0.078
	0.7	1.27±0.05^{a}	5.02±0.18^{a}		0.081
	0.8	8.99±0.34^{c}	9.41±0.33^{c}		0.097
	0.9	14.21±0.56^{d}	9.76±0.34^{c}		0.137
Vanillin/chitosan molar ratio (-)	0.0	1.11±0.05^^{a}	4.80±0.17^{a}	0.73	0.116
	0.3	2.05±0.08^{b}	5.90±0.21^{b}		0.108
	0.7	2.34±0.09^{c}	6.50±0.23^{c}		0.113
	1.3	1.78±0.07^{b}	5.15±0.18^{a}		0.081
Emulsifier	None (baseline)	1.27±0.05^{b}	5.02±0.18^{b}	0.73	0.081
	Tween 20®	0.37±0.02^{a}	3.56±0.12^{a}	0.79	0.052
	Tween 60®	0.36±0.01^{a}	3.41±0.12^{a}	0.80	0.061

Superscript letters (a,b,c,d) denote ANOVA groupings ($p < 0.05$); same letter = no significant difference between conditions within each variable.

Overall, the results indicate that the optimal processing conditions were achieved at 4.0 min and 9,500 rpm (τ_0 = 1.27 Pa, k = 5.02 Pa·s^{n}). Under these conditions, extended homogenization promoted structural development without inducing over-shearing.

3.2. Effect of Homogenization Speed

Emulsions were prepared following the standard two-stage emulsification process: initial mixing stage (3 min at 9,500 rpm) followed by homogenization stage. Homogenization speeds were varied at 6,500, 9,500, 13,500, and 17,500 rpm for a fixed duration of 4.0 min (selected from time effect results showing minimal time-dependent variation beyond 4 min), with orbital shaking maintained at 150 rpm.

3.2.1. Time Sweep

Time sweeps at constant shear rate (10 s^{-1}) confirmed emulsion stability, with all systems exhibiting linear behavior and no changes in viscosity during measurements up to 8 minutes. Apparent viscosity increased considerably with homogenization speed (6,500 to 17,500 rpm), consistent with smaller droplet sizes produced by higher shear intensities.

3.2.2. Strain Sweep

Strain sweeps (1 Hz) confirmed the LVR beyond 1% strain across all homogenization speeds tested. Both G′ and G′′ moduli remained constant throughout the strain range examined, with no significant stress-strain slope changes observed. The 1% strain amplitude was therefore appropriate for subsequent frequency sweep measurements.

 doi:10.20944/preprints202602.1360.v1

3.2.3. Frequency Sweep

Figure 2A shows frequency sweeps (1% strain) for emulsions prepared at different homogenization speeds. The G'' exceeded G' across the entire frequency range, consistent with previous observations. G' exhibited the characteristic slope change near 0.1 Hz, but differences between speeds were practically negligible. Slight G' separation occurred only at 17,500 rpm and very low frequencies, much less pronounced than time-dependent effects. This indicates homogenization speed primarily affects droplet size refinement rather than bulk network structure. Negligible differences across speeds indicate shear intensity primarily refines microstructure post-network formation, stabilizing rheology beyond 6,500 rpm. This robustness suits scalable processing for oleogel precursors.

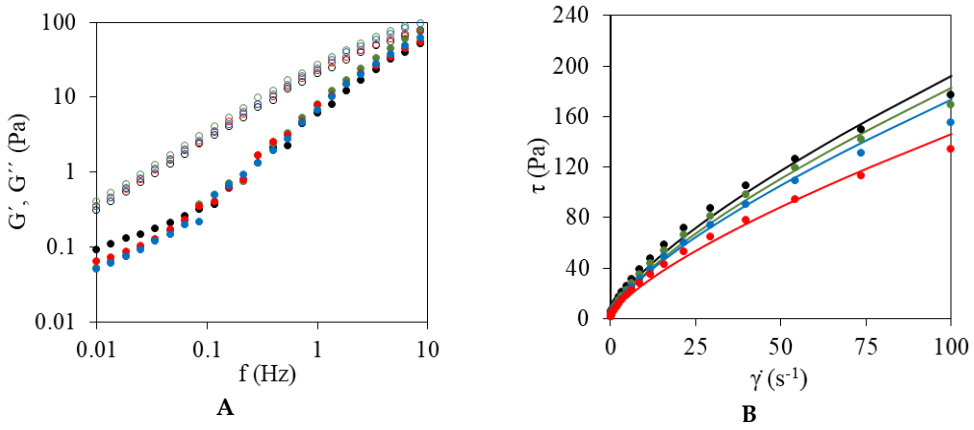

Figure 2. Effect of homogenization speed on rheological properties of olive oil–water emulsions. (A) Frequency sweep: storage (G', closed symbols) and loss (G'', open symbols) moduli. (B) Flow curves: shear stress (τ) versus shear rate (γ̇) with Herschel–Bulkley model fits (lines) overlaid on experimental data (dots). Conditions: 25 °C, 0.8% (w/v) chitosan, vanillin-to-chitosan molar ratio 0.7. Homogenization speeds: black (17,500 rpm), green (13,500 rpm), red (9,500 rpm), blue (6,500 rpm).

3.2.4. Flow Curves

Figure 2B shows flow curves from steady shear measurements, with Herschel-Bulkley parameters in Table 2. Flow behavior index remained constant at n = 0.73 across all speeds, confirming pseudoplastic behavior. Both consistency index (k from 5.92±0.21 to 6.54±0.23 Pa·s^n) and yield stress (τ_0 from 1.64±0.11 to 3.44±0.14 Pa) generally increased with homogenization speed (from 6,500 to 17,500 rpm), except at 9,500 rpm where unexpectedly lower values were determined. Model fits were acceptable (RMSE 0.059–0.121), with the poorest adjustment at the lowest speed (6,500 rpm). Apparent viscosity versus shear stress profiles (data not shown) exhibited the characteristic two-stage shear-thinning behavior observed for homogenization time effects: sharp initial viscosity decrease at low shear stresses followed by slope reduction at higher stresses, consistent with literature reports. From these findings, a processing speed above 6,500 rpm favored droplet refinement rather than changes in bulk rheology.

3.3. Effect of Reaction Temperature

Emulsions were maintained under magnetic stirring post-homogenization (4 min at 9,500 rpm) at temperatures of 25, 40, and 55 °C to promote chitosan-vanillin reaction (Schiff reaction). Higher temperatures were expected to enhance reaction extent and emulsion structuration while maintaining constant processing conditions (homogenization time and speed).

 doi:10.20944/preprints202602.1360.v1

3.3.1. Time Sweep

Time sweeps (10 s^{-1}) confirmed system stability across all temperatures, with no viscosity variations observed. Apparent viscosity increased with reaction temperature, supporting the hypothesis of enhanced structuration at higher temperatures.

3.3.2. Strain Sweep

Strain sweeps (1 Hz) confirmed LVR up to 1% strain across all temperatures. Notably, moduli values increased with temperature, particularly G′ showing greater sensitivity than in previous processing variables, indicating stronger network formation at higher reaction temperatures.

3.3.3. Frequency Sweep

Figure 3A shows frequency sweeps (1% strain) for emulsions reacted at 25, 40, and 55 °C. While viscous-dominant behavior (G′′>G′) persisted across all temperatures, significant variations appeared compared to previous processing variables. The characteristic G′ slope change near 0.1 Hz was dampened at higher temperatures (less pronounced at 40 °C, nearly absent at 55 °C). Both moduli increased systematically with temperature, most evident in G′′, with reduced separation between G′ and G′′ indicating lower damping factor. At 55 °C, G′ showed a steeper slope than G′′, suggesting proximity to gelation point (G′=G′′ crossover) at higher frequencies beyond the tested range. This reflects advanced chitosan-vanillin reaction kinetics favoring network densification.

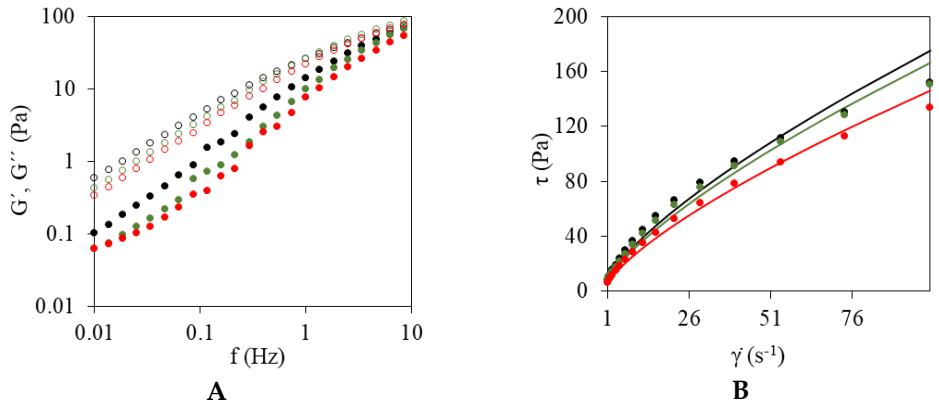

Figure 3. Effect of temperature on rheological properties of olive oil–water emulsions. (A) Frequency sweep: storage (G′, closed symbols) and loss (G′′, open symbols) moduli. (B) Flow curves: shear stress (τ) versus shear rate (γ̇) with Herschel–Bulkley model fits (lines) overlaid on experimental data (dots). Conditions: 13,500 rpm, 0.8% (w/v) chitosan, vanillin-to-chitosan molar ratio 0.7. Temperatures: black (55 °C), green (40 °C), red (25 °C).

3.3.4. Flow Curves

Figure 3B shows flow curves (experimental and Herschel-Bulkley fitted) for emulsions reacted at 25, 40, and 55 °C, with model parameters in Table 2. Flow behavior index (n=0.73) confirmed consistent pseudoplasticity. Both consistency index (k) and yield stress (τ_0) exhibited significant increases with reaction temperature (25 °C: τ_0=1.27±0.05 Pa, k=5.02±0.18 Pa·s^n; 55 °C: τ_0=2.71±0.11 Pa, k=5.99±0.21 Pa·s^n). Model fits were acceptable (RMSE 0.081–0.101, worst at 55 °C). Monotonic τ_0 and k rises reflect accelerated chitosan-vanillin Schiff base formation at higher temperatures.

3.3.5. Temperature Ramps

Temperature ramps assessed thermal stability via accelerated aging simulation for reaction temperature effects only (processing variables showed insufficient rheological differences). As shown in Figure 4, complex viscosity (|η*|) increased systematically with reaction temperature (25 < 40 ≈ 55 °C), reflecting enhanced chitosan-vanillin reaction and structuration. Post-thermal cycle analysis at

 doi:10.20944/preprints202602.1360.v1

25 °C showed the 25 °C emulsion exhibited slight viscosity decrease, indicating reduced stability and potential recoalescence risk. Conversely, 40 °C and 55 °C emulsions showed viscosity increases post-cycle (most pronounced at 40 °C), confirming greater thermal robustness and resistance to destabilization mechanisms. Higher reaction temperatures promote Schiff base formation, yielding emulsions with superior long-term stability against phase separation phenomena.

Overall, increasing the reaction temperature accelerated Schiff base formation (25–55 °C), leading to a 113% increase in yield stress (τ_0) and a dampened G′ slope. These effects resulted in enhanced thermal stability, as evidenced by viscosity increases after 50 °C [23].

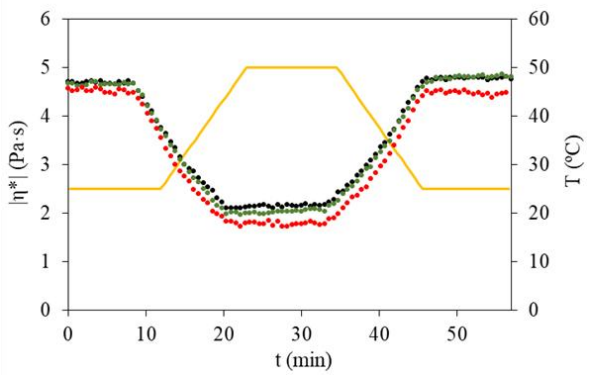

Figure 4. Effect of reaction temperature on thermal stability of olive oil–water emulsions. Temperature ramp: complex viscosity (|η*|) versus temperature. Conditions: 13,500 rpm, 0.8% (w/v) chitosan, vanillin-to-chitosan molar ratio 0.7. Temperatures: black (55 °C), green (40 °C), red (25 °C).

3.4. Effect of Chitosan Concentration

Emulsions were prepared at chitosan concentrations of 0.6, 0.7, 0.8, and 0.9% w/w (1.0% failed due to excessive aqueous phase viscosity preventing proper droplet breakup and phase mixing). Chitosan concentration influences continuous phase rheology and minimum achievable droplet size, affecting emulsion stability and flow behavior (Braginsky & Belevitskaya, 1996; McClements, 2005).

3.4.1. Time Sweep

Time sweeps (10 s^{-1}) confirmed stability across all concentrations, with no significant viscosity changes. Two distinct viscosity groups emerged: higher values (~7 Pa·s) for 0.8-0.9% chitosan vs lower values (~3 Pa·s) for 0.6-0.7%.

3.4.2. Strain Sweep

Strain sweeps (1 Hz) confirmed LVR up to 1% strain for all concentrations. Moduli formed two clear groups mirroring viscosity trends, with 0.8-0.9% showing substantially higher G′ and G′′ values, particularly pronounced for G′.

3.4.3. Frequency Sweep

Figure 5A shows frequency sweeps (1% strain, within LVR) for emulsions prepared at different chitosan concentrations. Both G′ and G′′ moduli formed two distinct groups: higher values at > 0.8% w/w chitosan vs lower values at < 0.7% w/w, with nearly identical trends and magnitudes within each pair. Higher concentrations (> 0.8% w/w) produced substantially elevated moduli compared to lower concentrations (< 0.7% w/w). G′ exhibited characteristic dual-slope behavior (inflection ~ 0.1 Hz), but dampened at higher concentrations, signaling suppressed transient flocculation via denser polymer bridging, enhanced interfacial coverage, and viscosity ratio shifts limiting minimum droplet size [24,25].

 doi:10.20944/preprints202602.1360.v1

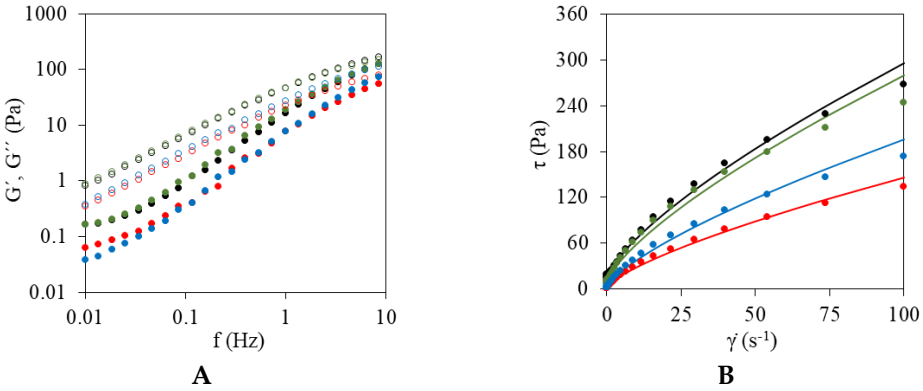

Figure 5. Effect of chitosan concentration on rheological properties of olive oil–water emulsions. (A) Frequency sweep: storage (G′, closed symbols) and loss (G′′, open symbols) moduli. (B) Flow curves: shear stress (τ) versus shear rate ($\dot{\gamma}$) with Herschel–Bulkley model fits (lines) overlaid on experimental data (dots). Conditions: 13,500 rpm, 25 °C, vanillin-to-chitosan molar ratio 0.7. Chitosan concentrations: black (0.9%), green (0.8%), red (0.7%), blue (0.6%) (w/v).

3.4.4. Flow Curves

Figure 5B and Table 2 present Herschel-Bulkley fits for chitosan concentration effects, with good RMSE (0.077-0.117) and constant shear-thinning index n = 0.73 across concentrations. The characteristic concentration pairs persisted in τ_0 (2.21→14.21 Pa) and K (5.02→9.76 Pa·s^n) with monotonic increases, except 0.6% > 0.7% inversion mirroring preliminary aqueous chitosan viscosities. Apparent viscosity vs shear stress confirmed steeper shear thinning at higher chitosan levels, consistent with polysaccharide stabilized emulsions. The yield stress τ_0 increased ~11 fold from 1.27 Pa (0.7%) to 14.21 Pa (0.9%), indicating a sharp reinforcement of the flocculated droplet network around 0.8–0.9% without evidence of a full liquid to solid viscoelastic transition. This concentration window likely reflects saturation of droplet surface coverage and enhanced polymer bridging, which markedly raises flow resistance but still preserves predominantly viscous behavior in the frequency domain.

3.4.5. Temperature Ramps

Temperature ramps revealed the same two-group structuring observed across prior tests, with high-concentration emulsions (> 0.8% w/w chitosan) exhibiting substantially higher complex viscosities than low-concentration ones (< 0.7% w/w) throughout programmed cycles.

Complex viscosity followed expected trends: high-chitosan emulsions showed nearly identical, elevated profiles, while low-chitosan pairs displayed similar, lower values. Pre/post-50 °C stability analysis confirmed overall consistency, at 0.6% w/w showing the greatest decline, 0.8% w/w minimal change, and 0.9% w/w slight increase—correlating greater structuring with enhanced thermal stability, consistent with temperature effects during emulsification.

Overall, the chitosan concentration exhibited a percolation threshold at approximately 0.8% w/w, leading to a marked increase in viscosity (from 3 to 7 Pa·s) and an eleven-fold escalation in yield stress (τ_0, from 1.27 to 14.21 Pa). This transition was accompanied by suppression of the G′ inflection near 0.1 Hz, reflecting reduced low-frequency relaxation which may due to enhanced interdroplet bridging at higher chitosan concentrations. Vanillin-chitosan reactions further promoted chain entanglement by disrupting chitosan crystallinity, consistent with acid-solubilized polysaccharides.

3.5. Effect of Vanillin/Chitosan Molar Ratio

Emulsions were prepared at fixed 0.7% w/w chitosan with vanillin/chitosan molar ratios of 1.3, 0.7, 0.3, and 0.0. This systematic variation isolated molar stoichiometry effects on cross-linking efficiency and emulsion rheology.

 doi:10.20944/preprints202602.1360.v1

3.5.1. Time Sweep

Time sweeps confirmed system stability across all ratios. Notably, the 0.7 ratio produced the highest viscosity, exceeding the vanillin-excess 1.3 ratio, while 0.3 and 0.0 ratios showed lower values.

3.5.2. Strain Sweep

Strain sweeps (1 Hz) verified LVR up to 1% strain for all formulations. The no-vanillin (0.0) sample exhibited substantially elevated moduli and stress compared to vanillin-containing systems, indicating baseline chitosan network reinforcement without cross-linking competition.

3.5.3. Frequency Sweep

Figure 6A shows frequency sweeps (1% strain, within LVR) for emulsions at fixed 0.7% w/w chitosan and varying vanillin/chitosan molar ratios. The G′ and G′′ moduli formed two distinct behavioral groups: 1.3/0.7 ratios (higher values, similar trends) vs 0.3/0.0 ratios (lower values). G′′ showed slight monotonic increase with rising vanillin ratio, while G′ exhibited pronounced differences between pairs. The characteristic dual-slope G′ behavior (~ 0.1 Hz inflection) sharpened at low ratios (maximal at 0.0, no cross-linking) but blurred near stoichiometry (1.3/0.7), as excess/unreacted vanillin disrupts optimal imine bridging and electrostatic structuring.

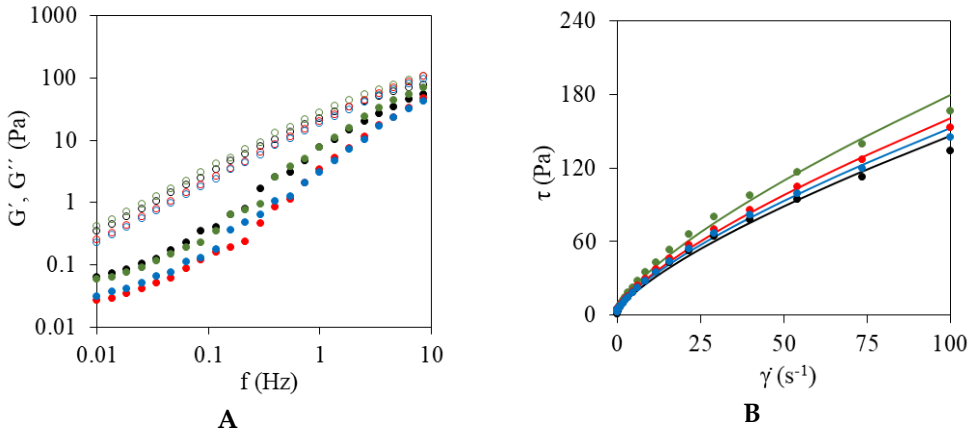

Figure 6. Effect of vanillin-to-chitosan molar ratio on rheological properties of olive oil–water emulsions. (A) Frequency sweep: storage (G′, closed symbols) and loss (G′′, open symbols) moduli. (B) Flow curves: shear stress (τ) versus shear rate (γ̇) with Herschel–Bulkley model fits (lines) overlaid on experimental data (dots). Conditions: 13,500 rpm, 25 °C, 0.8% (w/v) chitosan. Vanillin-to-chitosan molar ratios: black (1.3), green (0.7), red (0.3), blue (0).

3.5.4. Flow Curves

Figure 6B and Table 2 present Herschel-Bulkley fits for vanillin/chitosan ratio effects at fixed 0.7% w/w chitosan, with satisfactory correlation and constant shear-thinning index n = 0.73 (range 0.71-0.77). The τ_0 and K increased monotonically with increasing vanillin/chitosan ratio up to 0.7, but 1.3 excess vanillin yielded lowest values. Unreacted vanillin likely disrupts structuring by incomplete imine cross-linking, reducing emulsion stability as observed in frequency sweeps. Apparent viscosity vs shear stress exhibited characteristic steep shear-thinning zones transitioning to gentler slopes.

3.5.5. Temperature Ramps

Temperature ramps assessed thermal stability across vanillin/chitosan ratios at fixed 0.7% w/w chitosan. Complex viscosity profiles confirmed paired behaviors: 1.3/0.7 ratios (higher, similar values) vs 0.3/0.0 ratios (lower, converging trends). Viscosities after the 50 °C stage revealed low ratios (0.3/0.0) with slight declines (limited cross-linking); 1.3 continued declining (excess vanillin

 doi:10.20944/preprints202602.1360.v1

interference) while 0.7 increased slightly (optimal reaction), all reaching matched final values consistent with incomplete kinetics.

It can be concluded that the vanillin-to-chitosan stoichiometry was optimized at a ratio of 0.7, yielding maximal yield stress (τ_0 = 2.34 Pa) and storage modulus (G′). Deviations from this ratio, either excess (1.3) or deficiency (0.3), impaired crosslinking due to unreacted species or insufficient imine formation. Excess vanillin increased instability as incomplete reaction kinetics left unreacted molecules interfering with structural development, consistent with recent chitosan-vanillin oleogel studies [12].

3.6. Effect of Emulsifying Agents

Tween® 20 and Tween® 60 (0.7% w/w each) were tested in baseline formulation (0.7% w/w chitosan, 1.3 vanillin/chitosan ratio, 25 °C, 4 min/9500 rpm homogenization). Surfactants reduce interfacial tension, droplet size, and recoalescence via rapid adsorption and protective interfacial layers (Schubert & Armbruster, 1992; McClements, 2005).

3.6.1. Time Sweep

Time sweeps confirmed stability for all systems. Tween addition substantially lowered viscosity compared to control.

3.6.2. Strain Sweep

Strain sweeps (1 Hz) verified LVR to 1% strain across formulations. Tween emulsions showed similar trends with elevated G′, particularly at low frequencies, versus control.

3.6.3. Frequency Sweep

Figure 7A shows frequency sweeps (1% strain, within LVR) for Tween® 20/60 emulsions vs control. Surfactant addition markedly increased both G′ and G′′, with Tween® 60 > Tween® 20 relative to non-surfactant baseline. The characteristic dual-slope G′ behavior (inflection point, maximum G′/G′′ separation) observed across prior experiments disappeared completely with Tween surfactants yielded linear G′ profiles with steeper slopes versus baseline. Although G′′ predominated (viscous character), Tween emulsions showed elevated G′ and substantially reduced tan δ (particularly at low frequencies) indicating enhanced elastic structuring. This reflects Tween's rapid interfacial adsorption (HLB-dependent: Tween 60 > 20), finer droplets, and partial displacement of chitosan–vanillin bridging networks, stabilizing flocculation while promoting more uniform elasticity [25,26].

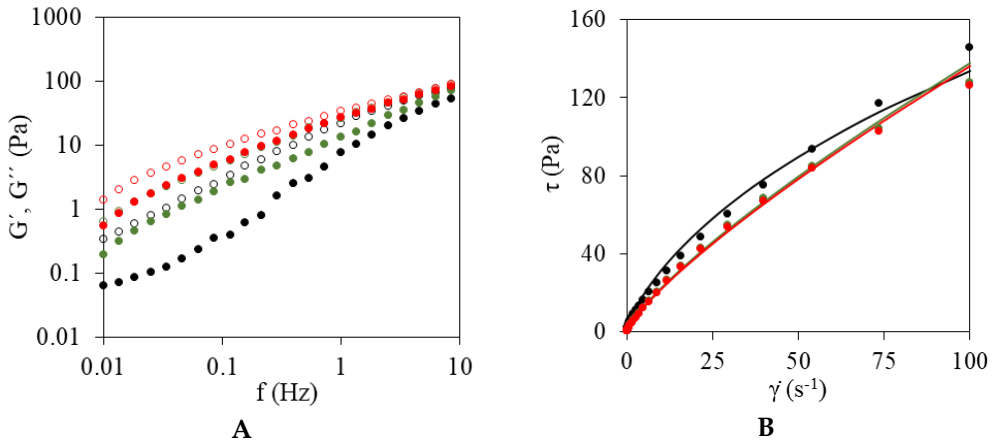

Figure 7. Effect of Tween emulsifier on rheological properties of olive oil–water emulsions. (A) Frequency sweep: storage (G′, closed symbols) and loss (G′′, open symbols) moduli. (B) Flow curves: shear stress (τ) versus shear rate ($\dot{\gamma}$) with Herschel–Bulkley model fits (lines) overlaid on experimental data (dots). Conditions: 13,500 rpm,

 doi:10.20944/preprints202602.1360.v1

25 °C, 0.8% (w/v) chitosan, vanillin-to-chitosan molar ratio 0.7. Emulsifiers: black (no Tween), green (Tween® 20), red (Tween® 60).

3.6.4. Flow Curves

Figure 7B and Table 2 present Herschel-Bulkley fits for Tween® 20/60 (0.7% w/w) vs control (baseline: 0.7% w/w chitosan, 1.3 vanillin/chitosan, 25 °C, 4 min/9500 rpm), confirming satisfactory adjustment across systems. Tween emulsions exhibited comparable viscosities substantially lower than control: τ_0 reduced from 2.34 Pa to 0.36-0.37 Pa (84%), K from 6.50 to 2.56-3.41 Pa·s^n (50-60%), with weakened shear-thinning character (n increased from 0.73 to 0.79-0.80)—marking the first oscillatory-rotational divergence across all variables. Apparent viscosity vs. shear stress showed attenuated steep decline (vs prior sharp transitions across variables) and absent initial low-slope regime vs control, confirming surfactant-modified yielding via competitive displacement of chitosan–vanillin networks despite finer droplets.

It can be highlighted that the incorporation of Tween® 20 and Tween® 60 led to a distinct divergence in rheological behavior. Oscillatory measurements showed enhanced viscoelasticity (increased G′/G′′, linear spectra, and near-gel convergence), whereas rotational tests revealed a pronounced structural collapse, with 84% reduction in yield stress (τ_0) and a shift toward more Newtonian behavior (n from 0.73 to 0.80). This contrast is attributed to competitive displacement of chitosan–vanillin interfacial films by non-ionic surfactants in an HLB-dependent manner (Tween® 60 > Tween® 20), which homogenized charge segregation and eroded the structured yield despite reduced droplet size (d_{32}). Among the surfactants, Tween® 20 exhibited slightly superior thermal robustness and overall improved emulsion performance across rheological assays [26]. Across all formulations, shear-tinning character was preserved (n ≈ 0.73, except in surfactant-containing emulsions), with consistent RMSE values and a characteristic two-stage apparent viscosity shear-thinning response. These features support a Pickering-like jamming mechanism in viscous-dominant systems (Φ = 0.52, G′′ > G′) (McClements, 2005). Temperature ramp tests further confirmed a strong correlation between structural development and stability, with optimal conditions identified at 0.9% w/w chitosan, a vanillin-to-chitosan ratio of 0.7, and 55 °C. Collectively, these results position the tunable, surfactant-free emulsions as promising precursors for marine oil oleogels, offering reduced flocculation sensitivity while delivering robust, gel-like functionality [21].

3.6.5. Temperature Ramps

Temperature ramps (1 Hz, 1% strain) assessed thermal stability for Tween® emulsions vs control. Complex viscosity (η^*) profiles revealed markedly elevated values for both Tween® 20/60 systems relative to non-surfactant baseline throughout thermal cycles.

Tween® 20 exhibited slightly higher η^* than Tween® 60, suggesting superior stability. Post-50 °C analysis confirmed: Tween® 20 uniquely increased η^* after thermal stress, while control and Tween® 60 showed declines—demonstrating Tween® 20's exceptional thermal robustness via enhanced interfacial stabilization [26].

4. Conclusions

The rheological characterization supported viscous-dominant behavior (G′′>G′) across all chitosan-vanillin emulsions at Φ = 0.52, consistent with literature precedents for concentrated emulsions below the jamming transition. A characteristic G′ slope inflection near 0.1 Hz—yielding maximum damping factor peaks—was universally observed except in Tween® surfactant emulsions, reflecting transient flocculation suppressed by crosslinking or interfacial saturation. Flow curves exhibited superimposable up/down sweeps, confirming absence of thixotropy or rheopexy, with acceptable Herschel-Bulkley model fits (n ≈ 0.73, 0 < n < 1) capturing shear-thinning across shear rates.

Homogenization time (4 min optimum) and speed (≥ 9,500 rpm) primarily refined microstructure without compromising stability, while reaction temperature (55 °C), chitosan

 doi:10.20944/preprints202602.1360.v1

concentration (~ 0.8-0.9% w/w percolation threshold), and vanillin/chitosan ratio (0.7 stoichiometric optimum) systematically enhanced yield stress, consistency index, and thermal robustness via accelerated Schiff base kinetics and network densification. Surfactant addition (Tween® 20 preferred over 60 for thermal stability) induced dual effects—oscillatory stiffening contrasting rotational softening through competitive interfacial displacement—yet reduced structured yield despite finer droplets.

Optimal protocol integrates 4 min homogenization at 9,500 rpm, 0.9% w/w chitosan, 0.7 vanillin/chitosan ratio, 55 °C reaction, yielding gel-like precursors for marine oil oleogels with suppressed flocculation and superior structuring versus conventional stabilization.

Author Contributions: Conceptualization, R.M. and D.F.; methodology, L.M.; formal analysis, D.R. data curation, L.M. and D.R.; writing—original draft preparation, L.M. and D.F.; writing—review and editing, L.M., D.R, R.M. and D.F.; funding acquisition, D.F. All authors have read and agreed to the published version of the manuscript.

Funding: This research was funded by MCIN/AEI/10.13039/501100011033 and, as appropriate, by the European Union Next Generation EU/PRTR (grant CNS2022-135217). Ramón Moreira and Daniel Franco belong to ED431B 2024/18 Grupo de Potencial Crecimiento funded by Xunta de Galicia (Spain).:

Data Availability Statement: The original contributions presented in this study are included in the article. Further inquiries can be directed to the corresponding author.

Conflicts of Interest: The authors declare no conflicts of interest.

References

1. López-Pedrouso, M.; Lorenzo, J.M.; Gullón, B.; Campagnol, P.C.B.; Franco, D. Novel Strategy for Developing Healthy Meat Products Replacing Saturated Fat with Oleogels. Curr. Opin. Food Sci. 2021, 40, 40–45. https://doi.org/10.1016/J.COFS.2020.06.003.
2. Miao, W.; Zhang, Z.; Lin, Q.; McClements, D.J.; Ji, H.; Jiang, L.; Wen, J.; Jin, Z.; Qiu, C. Preparation of Emulsion-Template Oleogels: Tuning Properties by Controlling Initial Water Content and Evaporation Method. Food Hydrocolloids 2025, 158, 110519. https://doi.org/10.1016/j.foodhyd.2024.110519.
3. Patel, A.R.; Rajarethinem, P.S.; Cludts, N.; Lewille, B.; De Vos, W.H.; Lesaffer, A.; et al. Biopolymer-Based Structuring of Liquid Oil into Soft Solids and Oleogels Using Water Continuous Emulsions as Templates. Langmuir 2015, 31, 2065–2073. https://doi.org/10.1021/la502829u.
4. Romoscanu, A.I.; Mezzenga, R. Emulsion-Templated Fully Reversible Protein-in-Oil Gels. Langmuir 2006, 22, 7812–7818. https://doi.org/10.1021/la060878p.
5. Martins, A.J.; Vicente, A.A.; Cunha, R.L.; Cerqueira, M.A. Edible Oleogels: An Opportunity for Fat Replacement in Foods. Food & Function 2018, 9, 758–773. https://doi.org/10.1039/c7fo01641g.
6. Halling, P.J.; Walstra, P. Protein-Stabilized Foams and Emulsions. Critical Reviews in Food Science and Nutrition 1981, 15, 155–203. https://doi.org/10.1080/10408398109527315.
7. Welch, C.F.; Rose, G.D.; Malotky, D.; Eckersley, S.T. Rheology of High Internal Phase Emulsions. Langmuir 2006, 22, 1544–1550.
8. Nie, C.Z.; Li, Y.; Huang, X.H.; Wang, H.P.; Wang, X.S.; Dong, X.P.; Zhu, B.W.; Qin, L. Multi-Scenario Application of Chitosan Emulsions as Fat Replacers: Based on the Regulation of Chitosan Hydrophobicity and Emulsion Rheological Properties. Food Hydrocolloids 2024, 155, 110237. https://doi.org/10.1016/j.foodhyd.2024.110237.
9. Paul, V.; Rai, D.C.; T.S., R.L.; Srivastava, S.K.; Tripathi, A.D. A Comprehensive Review on Vanillin: Its Microbial Synthesis, Isolation and Recovery. Food Biotechnology 2021, 35, 22–49. https://doi.org/10.1080/08905436.2020.1869039.
10. Lin, Q.; Wang, C.; Jin, Z.; Jiang, L.; Wen, J.; McClements, D.J.; Qiu, C. Construction of Oleogels Based on Emulsion Gels Stabilized by Glycyrrhizic Acid and Chitosan. Food Hydrocolloids 2024, 155, 110163. https://doi.org/10.1016/j.foodhyd.2024.110163.

 doi:10.20944/preprints202602.1360.v1

11. Nivetha, B.S.; Saravanan, M.; Thomas, P.E.; Vijayaraj, P.; Prabhasankar, P. Development of Chitosan-Based Oleogel Using Emulsion Template Approach: Characterization and Application as Fat-Replacer in Cookies. International Journal of Biological Macromolecules 2025, 292, 139130. https://doi.org/10.1016/j.ijbiomac.2024.139130.
12. Brito, G.B.; Peixoto, V.O.D.S.; Martins, M.T.; Rosário, D.K.; Ract, J.N.; Conte-Júnior, C.A.; et al. Development of Chitosan-Based Oleogels via Crosslinking with Vanillin Using an Emulsion-Templated Approach: Structural Characterization and Their Application as Fat-Replacer. Food Structure 2022, 32, 100264. https://doi.org/10.1016/j.foostr.2022.100264.
13. Zhao, W.; Li, Y.; Xue, C.; Wei, Z. Fabrication of Emulsion-Templated Oleogels with Whey Protein Isolate and Carboxymethyl Chitosan for Delivery of Antarctic Krill Oil. Food Research International 2025, 116611. https://doi.org/10.1016/j.foodres.2025.116611.
14. Brito, G.B.; Pinho-Jr, J.D.S.; Guimarães, A.D.S.; Conte-Júnior, C.A.; Nele, M.; Perrone, D.; Castelo-Branco, V.N. Optimization and Characterization of Crosslinked Chitosan-Based Oleogels Based on Mechanical Properties of Conventional Solid Fats. Polymers 2025, 17, 1526. https://doi.org/10.3390/polym17111526.
15. Zhu, J.; Tian, D.; Chen, X.; Huang, T.; Chen, X. Preparation of Chitosan–Phenolic Aldehyde Fragrance Oleogels and Comparative Study of Their Structure and Properties. Food and Bioprocess Technology 2024, 17, 4204–4242. https://doi.org/10.1007/s11947-024-03390-4.
16. Farooq, S.; Ahmad, M.I.; Zhang, Y.; Chen, M.; Zhang, H. Preparation, Characterization and Digestive Mechanism of Plant-Derived Oil Bodies-Based Oleogels Structured by Chitosan and Vanillin. Food Hydrocolloids 2023, 136, 108247. https://doi.org/10.1016/j.foodhyd.2022.108247.
17. Franco, J.M.; Berjano, M.; Guerrero, A.; Muñoz, J.; Gallegos, C. Flow Behaviour and Stability of Light Mayonnaise Containing a Mixture of Egg Yolk and Sucrose Stearate as Emulsifiers. Food Hydrocolloids 1995, 9, 111–121. https://doi.org/10.1016/S0268-005X(09)80273-7.
18. Tadros, T.F. Rheology of Dispersions: Principles and Applications. Weinheim: Wiley-VCH, 2010.
19. Samavati, V.; Emam-Djomeh, Z.; Mohammadifar, M.A.; Omid, M.; Mehdinia, A. Influence of Tragacanth Gum Exudates from Astragalus gossypinus on Rheological and Physical Properties of Whey Protein Isolate Stabilised Emulsions. International Journal of Food Science & Technology 2011, 46, 1636–1645. https://doi.org/10.1111/j.1365-2621.2011.02661.x.
20. Abdolmaleki, K.; Mohammadifar, M.A.; Mohammadi, R.; Fadavi, G.; Meybodi, N.M. The Effect of pH and Salt on the Stability and Physicochemical Properties of Oil-in-Water Emulsions Prepared with Gum Tragacanth. Carbohydrate Polymers 2016, 140, 342–348. https://doi.org/10.1016/j.carbpol.2015.12.081.
21. Abdolmaleki, K.; Alizadeh, L.; Nayebzadeh, K. Temperature Dependence of Stability, Steady and Dynamic Rheological Properties of Oil-in-Water Emulsions Stabilized by Gum Tragacanth. Journal of Food Measurement and Characterization 2019, 13, 1627–1635. https://doi.org/10.1007/s11694-019-00079-7.
22. Samavati, V.; Emam-Djomeh, Z.; Mohammadifar, M.A. Physical and Rheological Characteristics of Emulsion Model Structures Containing Iranian Tragacanth Gum and Oleic Acid. Journal of Dispersion Science and Technology 2013, 34, 1635–1645. https://doi.org/10.1080/01932691.2012.731645.
23. Hou, Z.; Gao, Y.; Yuan, F.; Liu, Y.; Li, C.; Xu, D. Investigation into the Physicochemical Stability and Rheological Properties of β-Carotene Emulsion Stabilized by Soybean Soluble Polysaccharides and Chitosan. Journal of Agricultural and Food Chemistry 2010, 58, 8604–8611. https://doi.org/10.1021/jf1015686.
24. Braginsky, L.M.; Belevitskaya, M.A. Kinetics of Droplets Breakup in Agitated Vessels. New York: Nova Science, 1996.
25. McClements, D. Food Emulsions: Principles, Practices and Techniques. Boca Raton: Taylor & Francis, 2005.
26. Schubert, H.; Armbruster, H. Principles of Formation and Stability of Emulsions. International Chemical Engineering 1992, 32.